



**UNIVERSITAT POLITÈCNICA DE CATALUNYA  
BARCELONATECH**

---

**Escola Tècnica Superior d'Enginyeria  
de Telecomunicació de Barcelona**

**DEPLOYABLE FRESNEL ZONE PLATE ANTENNA FOR  
CUBESATS – ELECTRICAL DESIGN**

**A Master's Thesis**

**Submitted to the Faculty of the  
Escola Tècnica d'Enginyeria de Telecomunicació de  
Barcelona**

**Universitat Politècnica de Catalunya**

**by**

**Adrián Márquez Alperi**

**In partial fulfilment  
of the requirements for the degree of  
MASTER IN TELECOMMUNICATIONS ENGINEERING**

**Advisor: Adriano José Camps Carmona**

**Barcelona, May 2021**





**Title of the thesis:** DEPLOYABLE FRESNEL ZONE PLATE ANTENNA FOR CUBESATS – ELECTRICAL DESIGN

**Author:** Adrián Márquez Alperi

**Advisor:** Adriano José Camps Carmona

## **Abstract**

CubeSats are no longer just an academic exercise, but they have become a commercial and technical solution in the space field. Improvements in miniaturization, electronics and energy have made it possible to reduce the dimensions of the spacecraft, and therefore, their antennas size. This document shows first the design and simulation of a deployable Fresnel Zone Plate type antenna. In a second stage, the manufacturing and testing is presented in two ways, using two configurations: a heavier and more robust one with a paint-based conductor and a lighter one with a silver adhesive tape-based conductor. Both results are positive, the second one being especially satisfactory and leading to subsequent studies that further improve the system.



Dedication: I would like to dedicate this project to Justo Márquez and Sonia Alperi, my parents, for educating me, helping me and advising me throughout my life, and without whom, I could not be performing this project.



## **Acknowledgements**

First of all, I would like to acknowledge Professor Adriano Camps for being my mentor, not only in this project, but in all the steps that I have been taking in my career. Secondly, to all the Nanosat Lab staff for helping me move forward with the project and answering any questions I may had. I would also like to thank Professor Sebastian Blanch for his help in the project measurements. Finally, I want to thank all the professors of the Universitat Politècnica de Catalunya and Universidad de Oviedo for transmitting all the knowledge without it, I could not have carried out this project.

## Revision history and approval record

| Revision | Date       | Purpose           |
|----------|------------|-------------------|
| 0        | 01/11/2020 | Document creation |
| 1        | 03/05/2021 | Document revision |
| 2        | 14/05/2021 | Document revision |
| 3        | 18/05/2021 | Document revision |

| Written by: |                       | Reviewed and approved by: |                            |
|-------------|-----------------------|---------------------------|----------------------------|
| Date        | 18/05/2021            | Date                      | 18/05/2021                 |
| Name        | Adrián Márquez Alperi | Name                      | Adriano José Camps Carmona |
| Position    | Project Author        | Position                  | Project Supervisor         |



## **Table of contents**

|  |    |
|--|----|
| Abstract .....   | 1  |
| Acknowledgements .....   | 3  |
| Revision history and approval record.....                          | 4  |
| Table of contents .....  | 5  |
| List of Figures .....  | 7  |
| List of Tables .....   | 9  |
| 1. Introduction.....   | 10 |
| 1.1. The CubeSat Standard.....                                     | 10 |
| 1.2. Deployable Antennas for CubeSats.....                         | 10 |
| 2. State of the art.....   | 12 |
| 2.1. Fresnel Zone Plate at Optical Wavelengths.....                | 12 |
| 2.2. Fresnel Zone Plate at Microwave Frequencies.....              | 12 |
| 3. Methodology and Design.....                                     | 14 |
| 3.1. Fresnel Zone Plate Design.....                                | 14 |
| 3.2. Feeder Design.....  | 16 |
| 4. Electromagnetic Analysis.....                                   | 17 |
| 4.1. Feeder Electromagnetic Analysis.....                          | 17 |
| 4.2. Fresnel Zone Plate Electromagnetic Analysis.....              | 17 |
| 4.2.1. Fresnel Zone Plate – Number of Zones Analysis.....          | 18 |
| 4.2.2. Fresnel Zone Plate - Focal Distance Variation Analysis..... | 19 |
| 4.2.3. Fresnel Zone Plate – Last Zone Radius Analysis.....         | 21 |
| 4.2.4. Fresnel Zone Plate – Mass Plane Analysis.....               | 22 |
| 4.2.5. Fresnel Zone Plate – Serrated Edge Last Zone.....           | 24 |
| 5. Fresnel Zone Plate Antenna Manufacturing.....                   | 26 |
| 5.1. Scaled Design and Electromagnetic Simulation.....             | 26 |
| 5.1.1. Calculation of Fresnel Zone Radius.....                     | 26 |
| 5.1.2. Fresnel Zone Plate Electromagnetic Analysis.....            | 26 |
| 5.2. Base Design.....  | 27 |
| 5.3. Rod Placement.....  | 28 |
| 5.4. Upper Triangle.....   | 28 |
| 5.4.1. Configuration A.....  | 28 |
| 5.4.2. Configuration B.....  | 29 |
| 6. Electromagnetic Measurements .....                              | 30 |



|      |  |    |
|------|--|----|
| 6.1. | Feeder Electromagnetic Measurement ..... | 30 |
| 6.2. | Configuration A - Measurement .....      | 31 |
| 6.3. | Configuration B - Measurement .....      | 32 |
| 7.   | Conclusions .....                        | 33 |
| 7.1. | Electromagnetic Conclusions .....        | 33 |
| 7.2. | Future Lines .....                       | 34 |
| 7.3. | Learned Lessons .....                    | 35 |
| 8.   | Budget .....                             | 36 |
| 9.   | Gantt Diagram .....                      | 37 |
|      | Bibliography .....                       | 38 |
|      | Glossary .....                           | 39 |

## **List of Figures**

|   |    |
|---|----|
| Figure 1. Different Forms of U Assembling. ....   | 10 |
| Figure 2. Auriga Spacecraft [2] .....   | 10 |
| Figure 3. Reflector Configurations for UPC NanoSat Lab Radiometer. (a) Regular Circular Mesh. (b) Irregular Standard Mesh. [6] .....                                | 11 |
| Figure 4. Zone Plate of Van Buskirk and Hendrix. [9].....   | 12 |
| Figure 5. Huygens Principle.....  | 14 |
| Figure 6. Fresnel Zone Plate of 20 Zones.....   | 15 |
| Figure 7. Feed antenna views. (a) Top view. (b) Side View. ....   | 16 |
| Figure 8. Simulated Return losses ( $S_{11}$ ) of the Feeder.....   | 17 |
| Figure 9. Simulated Radiation Pattern of the Feeder. ....   | 17 |
| Figure 10. FZP Number of Zones Analysis. ....   | 18 |
| Figure 11. Radiation Pattern for the 4-zoned Fresnel Zone Plate.....  | 18 |
| Figure 12. Evolution of the Directivity with the Distance Feeder-Plate Variation.....   | 19 |
| Figure 13. Radiation Pattern for the 4-zoned Fresnel Zone Plate at 580 mm away of the Feeder.....   | 20 |
| Figure 14. Evolution of the Directivity with the Last Zone Radius Variation.....  | 21 |
| Figure 15. Radiation Pattern for the 4-zoned Fresnel Zone Plate at 580 mm away of the Feeder and 30 mm more of Radius. ....   | 21 |
| Figure 16. Evolution of the Directivity with a Mass Plane. ....   | 22 |
| Figure 17. Radiation Pattern for the 4-zoned Fresnel Zone Plate at 580 mm away of the Feeder and 30 mm more of Radius with Circular/Square Mass Plane .....         | 23 |
| Figure 18. Diffracted Rays from a Reflector [12]. ....  | 24 |
| Figure 19. Fresnel Zone Plate with Serrated Edge. (a) Top View. (b) Side View.....  | 24 |
| Figure 20. Radiation Pattern for the 4-zoned Fresnel Zone Plate at 580 mm away of the Feeder and 30 mm more of Radius with Square Mass Plane and serrated edge..... | 25 |
| Figure 21. Radiation Pattern for the Prototype Fresnel Zone Plate. ....   | 26 |
| Figure 22. Fresnel Zone Plate Structure Design. ....  | 27 |
| Figure 23. Elevation of the Base.....   | 27 |
| Figure 24. Views of the Union. (a) Side View. (b) Top View. ....  | 28 |
| Figure 25. Upper Polystyrene Triangle. ....   | 29 |
| Figure 26. Configuration A - Assembled Antenna .....  | 29 |
| Figure 27. Configuration B - Assembled Antenna .....  | 29 |
| Figure 28. Feeder Measurement.....  | 30 |
| Figure 29. Feeder Measurement Results.....  | 30 |



Figure 30. Configuration A – Antenna Anchored in the Chamber.....31

Figure 31. Configuration A – Antenna Pattern Measurement.....31

Figure 32. Configuration B – Antenna Anchored in the Chamber.....32

Figure 33. Configuration B – Antenna Pattern Measurement.....32

Figure 34. Electromagnetic vs Measurement Farfield Results .....33

Figure 35. Metallic Material Comparison.....34

Figure 36. Gantt Diagram .....37

## **List of Tables**

|  |    |
|--|----|
| Table 1. Fresnel Zone Radius.....  | 15 |
| Table 2. $b_1$ and $b_2$ variation with $F_2$ Variation .....  | 15 |
| Table 3. Simulated Farfield Parameters for the 4-zoned Fresnel Zone Plate. ....  | 19 |
| Table 4. Simulated Farfield Parameters for the 4-zoned Fresnel Zone Plate at 580 mm away of the Feeder. ....   | 20 |
| Table 5. Simulated Farfield Parameters for the 4-zoned Fresnel Zone Plate at 580 mm away of the Feeder and 30 mm more of Radius. ....  | 22 |
| Table 6. Simulated Farfield Parameters for the 4-zoned Fresnel Zone Plate at 580 mm away of the Feeder and 30 mm more of Radius with Circular/Square Mass Plane. ....          | 23 |
| Table 7. Simulated Farfield Parameters for the 4-zoned Fresnel Zone Plate at 580 mm away of the Feeder and 30 mm more of Radius with Square Mass Plane and serrated edge. .... | 25 |
| Table 8. Prototype Fresnel Zone Radius.....  | 26 |
| Table 9. Simulated Farfield Parameters for the Prototype Fresnel Zone Plate. ....  | 27 |
| Table 10- Configuration A – Antenna Pattern Measurement Parameters Results .....   | 31 |
| Table 11- Configuration B – Antenna Pattern Measurement Parameters Results .....   | 32 |
| Table 12- Electromagnetic vs Measurement Parameters Results .....  | 33 |
| Table 13. Materials Budget.....  | 36 |
| Table 14. Measurement Equipment Budget.....  | 36 |
| Table 15. Engineers Salary Break Down .....  | 36 |
| Table 16. Budget of the Whole Project .....  | 36 |

## 1. Introduction

### 1.1. The CubeSat Standard

CubeSat is a de facto standard for nanosatellites, and, nowadays, for small microsatellites as well, characterized by its small size and weight. It was created in 1999 by professors Jordi Puig-Suari, from California Polytechnic State University and Bob Twiggs, from Stanford University. Although this kind of standard was originally created for educational purposes, increasing the accessibility to space to students, it has become an attractive alternative to some larger spacecraft missions. The CubeSat standard defines a unit satellite, called 'U'. A unit is a cube of 10 cm with a mass no larger than 2 kg. Nevertheless, although a 'U' can be fully self-sufficient and be launched into orbit, it is common to group units, obtaining a range of satellites from 1U to 12U (Figure 1.). [1]

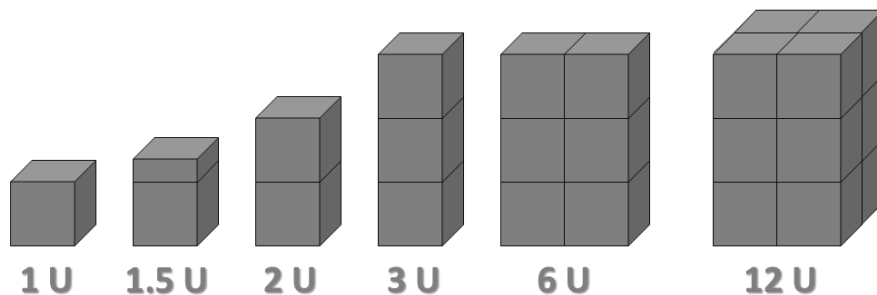


**Figure 1. Different Forms of U Assembling.**

Furthermore, several companies, like Dauria Aerospace are expanding the standard, designing the "Auriga" (Figure 2), a 16U designed for Earth surface imaging in 5 spectral bands with 2.5 m GSD from a circular SSO 600 km [2].

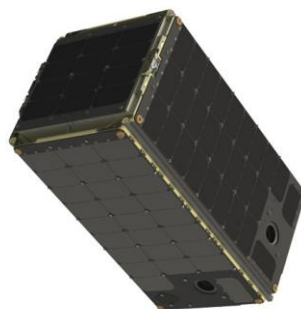


**Figure 2. Auriga Spacecraft [2]**

### 1.2. Deployable Antennas for CubeSats

One of the most important parts in a satellite is the communications subsystem, which is in charge of communicating the spacecraft with another system, either a ground station or another satellite using electromagnetic signals transmitted and received by the antennas.

Deployable parabolic reflector antennas are receiving an increased interest in CubeSats, among other things, because of their large gain, which allows to transmit less power, and allows the satellite to transmit or receive waves from one specific direction only.

Several types of deployable reflectors have been used in spacecraft. In 1974, the first large deployable antenna was launched. It was part of the ATS-6, whose deployable parabolic antenna had more than 9 meters in diameter [3]. Since ATS-6, several deployable methods and configurations have been studied. However, although there are few CubeSat missions that uses deployable antennas, the rapid evolution of the standard and its size and weight characteristics, are booming the development of compact deployable antennas, appearing several proposals that use dishes from 1 to 3 m of diameter. [4]

The UPC NanoSat Lab [5] is currently in the design phase of a mission to measure surface soil moisture with a microwave radiometer at L-Band (1.413 GHz). The first approach was a Deployable Offset Reflector into a 12 U CubeSat. Two configurations were studied, a regular circular mesh configuration and a standard irregular mesh configuration (Figure 3) [6].

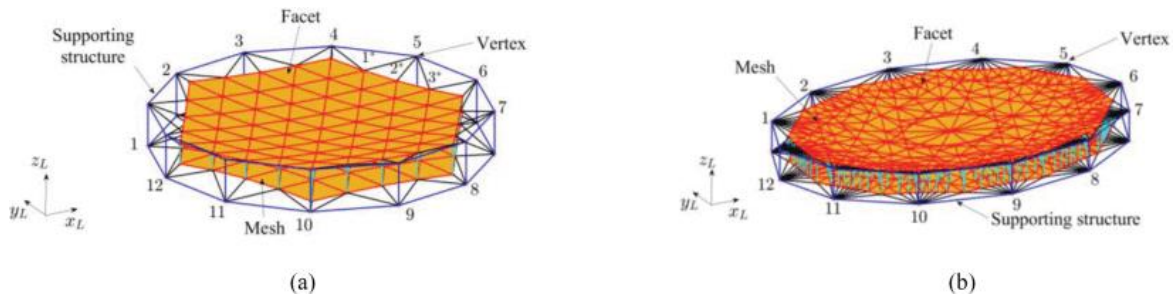


**Figure 3. Reflector Configurations for UPC NanoSat Lab Radiometer. (a) Regular Circular Mesh. (b) Irregular Standard Mesh. [6]**

The Regular Circular Mesh had 169 nodal points, while the Irregular Standard Mesh configuration had 301 nodal points. However, they had the same effective surface, 1 m<sup>2</sup> [6].

Nevertheless, the structural complexity of the system, and the lack of space into the 12 U CubeSat forced to study a more compact and easy to deploy alternative. This document shows a different option to enhance the directivity of the antenna using another deployable technology, a Fresnel Zone Plate.

## 2. State of the art

### 2.1. Fresnel Zone Plate at Optical Wavelengths

Fresnel Zone Plates evolved from the ideas on interference and diffraction of light of Augustin Fresnel, who showed that light from contiguous zones had  $180^\circ$  phase change. Then, John William Strutt, 3<sup>rd</sup> Baron Rayleigh and 1904 Nobel Prize of Physics, discovered that blocking light in alternative zones enhanced light in the center. In 1875 Jacques-Louis Soret designed a 98 zoned plate, alternating black and blacked-out circles, but it was Robert W. Wood who improved this plate obtaining a four-fold improvement effect at the focal point. [7]

### 2.2. Fresnel Zone Plate at Microwave Frequencies

The first mention of the use of a Fresnel Zone Plate at microwave frequencies was in 1936 in the United States by A. G. Clavier and R. H. Darbord, at a frequency around 1.5 GHz. Since that moment several patents were made, including several developments, like phase-correcting zone plates, allowing part of the energy intercepted by the openings to be efficiently focused on the feeder. [7].

In 1939, Bell Telephone Labs [8] discussed for the first time about using dielectric materials (titanium dioxide in rubber) of  $\epsilon_r=20$ , in order to avoid surface reflections. The design worked at 3 GHz, and the high value of the dielectric constant was decided in order to reduce the thickness and weight of the plate.

Later, in 1960 Sobel and Witse tested a new type of configuration performing off-axis fed plates, becoming this configuration really typical at millimeter wavelengths transmissions due to its accurate phase corrections. [8]

Then, in 1961 several attempts to improve phase correction were made, highlighting the design of Van Buskirk and Hendrix (Figure 4), whose plate consisted of a transmission half-open zone and a reflective half-open zone plate backed by a reflector spaced a quarter wavelength away at X-Band, demonstrating the simplicity of manufacturing the system, and opening the way to applications where large aperture focusing elements are required, such as low cost and space radio telescopes and communications antennas [9].

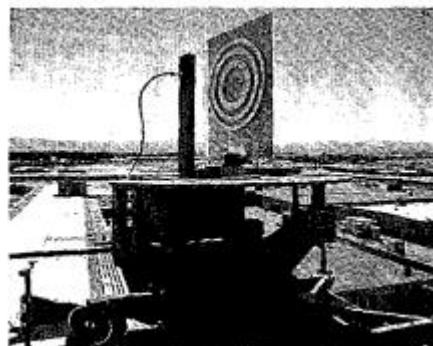


Figure 4. Zone Plate of Van Buskirk and Hendrix. [9]



In 1968, Sanyal and Singh measured, at several frequencies at X-Band, the axial and transverse variations of the focal region. Nevertheless, the zone plate was fabricated incorrectly, obtaining unfortunate results although the theoretical phase corrections were successful [6].

In the last 50 years, several developments have occurred in this field around the world in optical telescopes or satellite, purposes between others, hand in hand with international research groups improve the efficiency of this technology, which has reached a new level of development [7].

### 3. Methodology and Design

#### 3.1. Fresnel Zone Plate Design

From the Huygens principle [10], it is known that any point of a wavefront, can be considered as a source of new waves that expand from that point (Figure 5). Having said that, Fresnel theory states that, having 2 two antennas, positioned in two points, A and B, and working one of them as transmitter and the other one as receiver, the transmitted waves can travel directly from A to B in a straight line, or can arrive to the receiver following other longer paths path that introduce an additional phase shift with respect the direct beams which, in some cases it is destructive, giving place to the cancellation of the waves. Nevertheless, the reflection can also cause that the waves arrive in phase at the receiver, enhancing the received wave. This way, Fresnel Zone equation allows to calculate the dimension of the constructive zones.

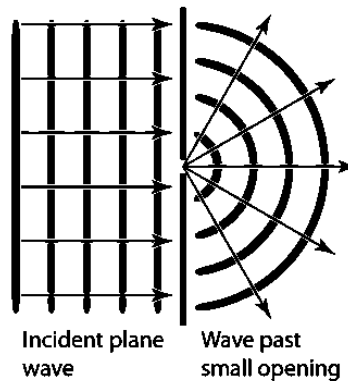


Figure 5. Huygens Principle.

As said before, Fresnel Zone Plates are made by several zones, that can be obtained with the Fresnel Zone equations (1).

$$b(n) = \sqrt{\frac{n\lambda F_1 F_2}{F_1 + F_2}} \quad n = 1 \dots N, \quad (1)$$

where

- $n$  is the number of the zone,
- $N$  is the total number of zones,
- $b$  is the radius of the  $n^{\text{th}}$  zone,
- $\lambda$  is the electromagnetic wavelength, and
- $F_1$  and  $F_2$  are the focal lengths.

Due to the lack of space inside the spacecraft, the plate has to be folded inside the CubeSat and it will be deployed once the satellite is in orbit. For that reason, the selected Fresnel Zone Plate will be totally flat, alternating concentric metallic zones with dielectric ones.

Having said that, the radius of the Fresnel zones (1) are shown in Table I. Nevertheless, several parameters must be defined before the calculation of the radius:

- $N = 20$
- $\lambda = \frac{c}{f} = \frac{3 \cdot 10^8}{1.413 \cdot 10^9} = 212.31 \text{ mm}$
- $F_1 = 0.75 \text{ m}$
- $F_2 = 500 \text{ km}$

It is important to remark that  $F_1$ , was selected after a previous dimension study in order to achieve a possible deployable antenna that could fit inside the spacecraft. On the other hand,  $F_2$ , that is the satellite height, was set to 500 km, however, at long distances, the variation of the zones is negligible, being possible a higher or lower satellites heights like the example of Table 2 shows.

**Table 1. Fresnel Zone Radius.**

| $n$      | 1      | 2      | 3      | 4      | 5      | 6      | 7      | 8      | 9      | 10     |
|----------|--------|--------|--------|--------|--------|--------|--------|--------|--------|--------|
| $b$ [mm] | 399.0  | 564.3  | 691.2  | 798.1  | 892.3  | 977.4  | 1055.8 | 1128.7 | 1197.1 | 1261.9 |
| $N$      | 11     | 12     | 13     | 14     | 15     | 16     | 17     | 18     | 19     | 20     |
| $b$ [mm] | 1323.5 | 1382.3 | 1438.8 | 1493.1 | 1545.5 | 1596.2 | 1645.3 | 1693.0 | 1739.4 | 1784.6 |

**Table 2.  $b_1$  and  $b_2$  variation with  $F_2$  Variation**

| $F_2$ [km] | 400      | 500      | 600      |
|------------|----------|----------|----------|
| $b_1$ [mm] | 399.0431 | 399.031  | 399.0432 |
| $b_2$ [mm] | 564.3321 | 564.3322 | 564.3323 |
| $b_3$ [mm] | 691.1629 | 691.1630 | 691.1631 |
| $b_4$ [mm] | 798.0861 | 798.0863 | 798.0864 |

Once the radii of the zones have been obtained, the plate can be implemented, being air the dielectric in the even zones, and metal the odd ones (Figure 6) in order to obtain a sum in phase of all the waves that arrive to/from the plate.

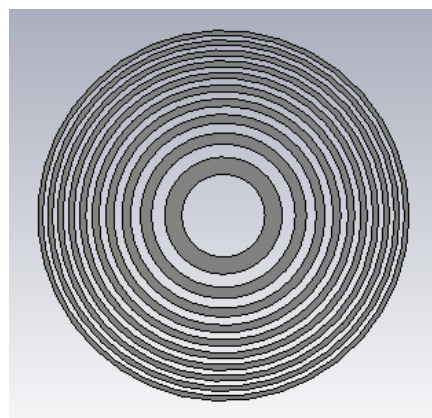


**Figure 6. Fresnel Zone Plate of 20 Zones.**

### 3.2. Feeder Design

Due to its simplicity, weight, volume and reduced back radiation, the feeder of the antenna will be a patch radiating at 1.413 GHz placed at the top of the CubeSat and fed with a probe (Figure 7).

Rogers RT5880 ( $\epsilon_r=2.2$ ,  $tg_d=0.0009$ ), with a thickness of 3.175 mm is used as substrate. The patch dimensions are 67.75 x 67.75 mm while the probe is 10.83 mm away from the center for a 50- $\Omega$  matching. In addition, the size of the ground plane is limited to 94 mm x 94 mm, which is the internal size of the CubeSat PCBs (PC/104PCB form factor).

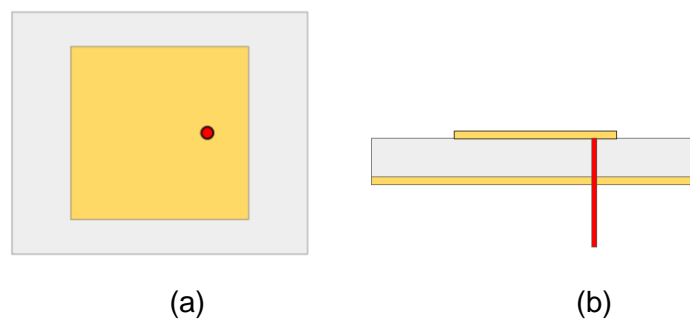


**Figure 7. Feed antenna views. (a) Top view. (b) Side View.**

## 4. Electromagnetic Analysis

It is important to remark that all the electromagnetic simulations have been performed using CST Studio Suite [11].

### 4.1. Feeder Electromagnetic Analysis

Figure 8 shows the simulation results for the patch. The patch is tuned at 1413 MHz and the return losses ( $S_{11}$ ) are smaller than -10 dB over a bandwidth of 27.6 MHz. On the other hand, Figure 9 shows the radiation pattern of the patch, which reaches a directivity of 7.11 dB.

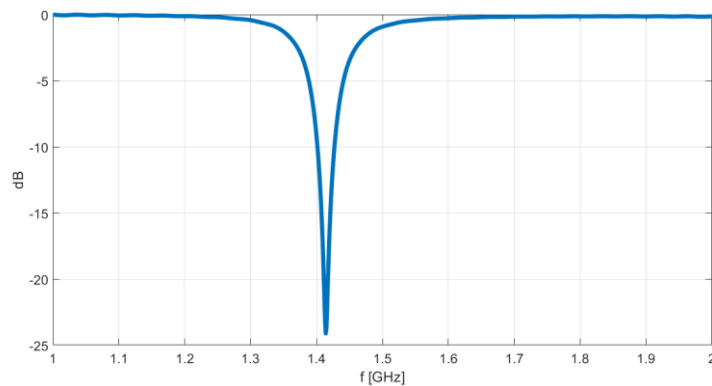


Figure 8. Simulated Return losses ( $S_{11}$ ) of the Feeder.

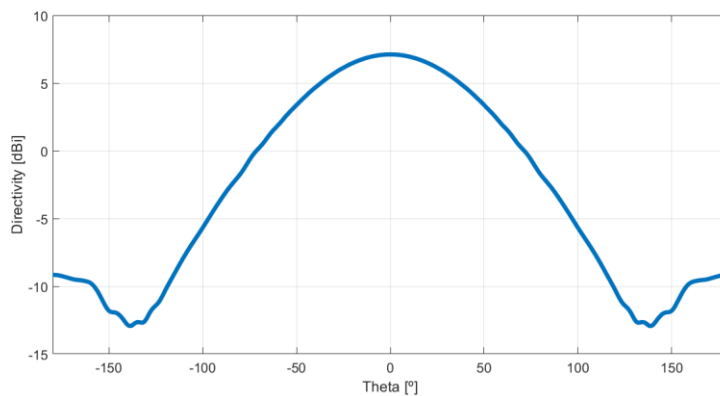


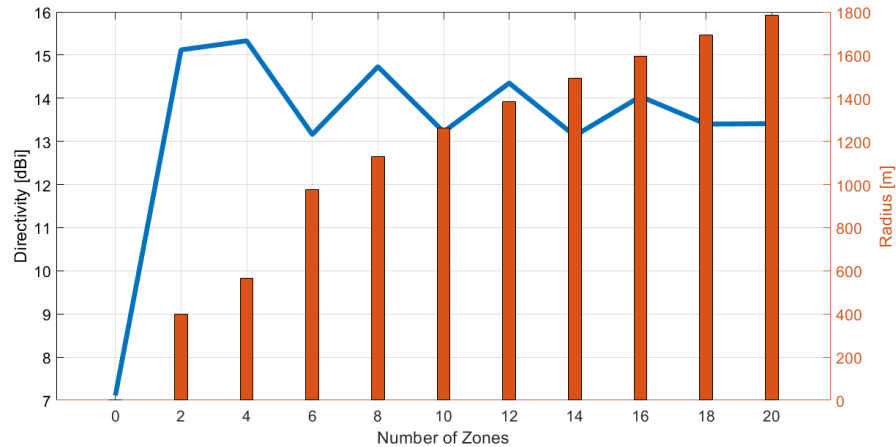
Figure 9. Simulated Radiation Pattern of the Feeder.

### 4.2. Fresnel Zone Plate Electromagnetic Analysis

Although the radii of the zones have been calculated for  $N=20$  zones, the lack of space inside the CubeSats forces to analyse a trade of between the directivity and the number of zones, the focal distance, and length of each radius.

### 4.2.1. Fresnel Zone Plate – Number of Zones Analysis

Since the size of the plate is really critical due to the lack of space inside the CubeSat, the directivity of the system for several  $N$  will be analysed (Figure 10). It is important to remark that only odd values of  $N$  will be used since even ones have their last plate made of air.



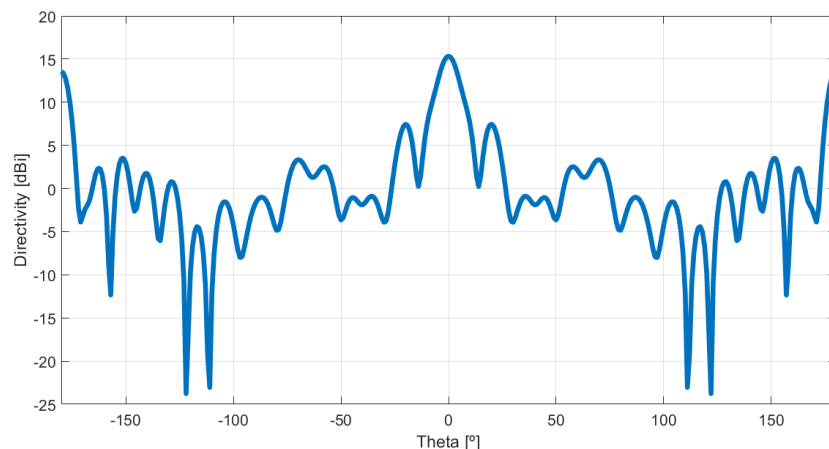
**Figure 10. FZP Number of Zones Analysis.**

Figure 10 shows relevant results. It can be seen that, unlike typical reflector configurations, where, the larger is the surface, the higher is the directivity. With this Fresnel Zone Plate, the maximum directivity enhancement is reached for  $N=4$  Zones.

From  $N=4$ , the directivity begins to decline between relative maxima and minima, always smaller than the maximum directivity reached with  $N=4$  Zones.

This result is really interesting and useful since it also means saving space inside the CubeSat with a smaller plate. Thus, the following analysis will be performed for a 4 zones plate.

Figure 11 shows the radiation pattern of the 4-zoned Fresnel Zone Plate, while Table 3 summarizes the main results of the plate.



**Figure 11. Radiation Pattern for the 4-zoned Fresnel Zone Plate.**

**Table 3. Simulated Farfield Parameters for the 4-zoned Fresnel Zone Plate.**

| <i>Parameter</i>                  | <i>Result</i> |
|-----------------------------------|---------------|
| <i>Directivity [dBi]</i>          | 15.33         |
| <i>Side Lobe Level. wrp. [dB]</i> | 7.88          |
| <i>F/B Ratio [dB]</i>             | 1.77          |
| <i>Radiation Efficiency [%]</i>   | 94.8          |

Results show that this kind of Plates increase the directivity by 8.22 dB. In addition, the SSL is 7.88 dB with respect the peak and the radiation efficiency of 94.8%. On the other hand, the most problematic parameter is the F/B Ratio, with a value of 1.77 dB, which means a large quantity of wasted radiation.

A possible solution to avoid the problem caused by the low front to back ratio is adding an absorbing material in order to avoid reflections on the back part of the plate towards the rear.

#### 4.2.2. Fresnel Zone Plate - Focal Distance Variation Analysis

In this section the defocusing of the plate with respect the feeder will be analysed and how it affects the efficiency of the system. To simulate this, the plate will be displaced farther away or closer to the focus on the axis that joins the feeder and the plate.

Figure 12 shows the evolution of the directivity with the variation of the distance between the feeder and the plate.

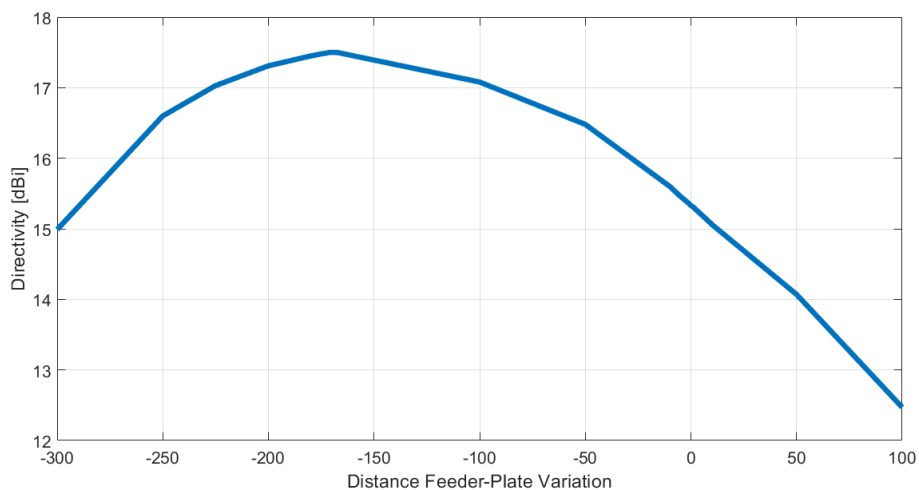


**Figure 12. Evolution of the Directivity with the Distance Feeder-Plate Variation.**

On the one hand, it can be seen that, as the distance between the feeder and the plate increases, the directivity decreases. On the other hand, as the feeder approaches the feeder, the directivity increases until around 17.5 dB where it starts to decrease again.

That point is reached at a variation of -170 mm, that is, a distance Feeder-Plate of 580 mm. Figure 13 shows the farfield obtained at that distance point, while Table 4 summarizes the main results of the system.

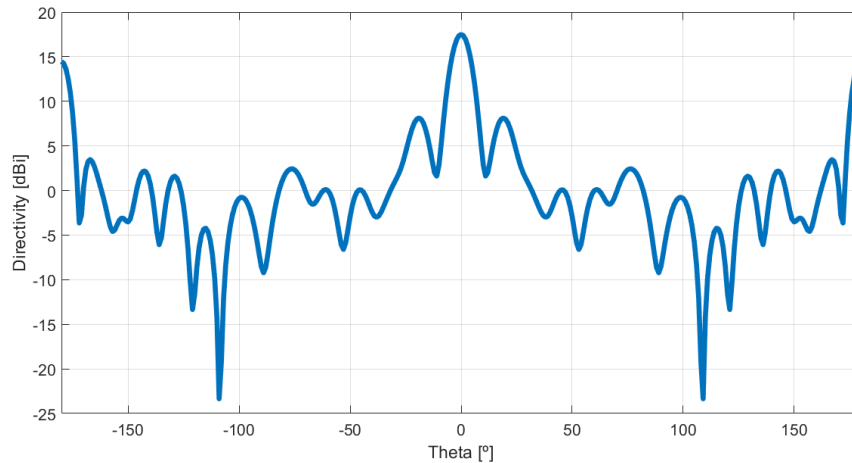


**Figure 13. Radiation Pattern for the 4-zoned Fresnel Zone Plate at 580 mm away of the Feeder.**

**Table 4. Simulated Farfield Parameters for the 4-zoned Fresnel Zone Plate at 580 mm away of the Feeder.**

| <i>Parameter</i>                  | <i>Result</i> |
|-----------------------------------|---------------|
| <i>Directivity [dBi]</i>          | 17.50         |
| <i>Side Lobe Level. wrp. [dB]</i> | 9.37          |
| <i>F/B Ratio [dB]</i>             | 3.25          |
| <i>Radiation Efficiency [%]</i>   | 93.8          |

Results show that approaching the plate to the feeder greatly improves the parameters with respect the original configuration (with a distance feeder-plate of 750 mm). Thus, directivity is enhanced 2.17 dBi, and the Side Lobe Level and the F/B Ratio is increased 1.485 dB and 1.48 dB respectively. On the other hand, radiation efficiency is slightly decreased by 0.95 %. Nevertheless, this loss in efficiency is negligible with respect to the rest of the improvements. Moreover, approaching the plate to the feeder, and therefore, to the CubeSat, facilitates the manufacturing of the antenna, and saves space inside the spacecraft in order to use it as a payload.

Thus, the subsequent analysis will be performed with a 4 Zones plate 580 mm away from the feeder.

### 4.2.3. Fresnel Zone Plate – Last Zone Radius Analysis

In this section, the behaviour of the system with respect to the variation of the radius of the last zone of the plate will be analysed. Figure 14 shows the evolution of the directivity with the variation of the radius of the last plate.

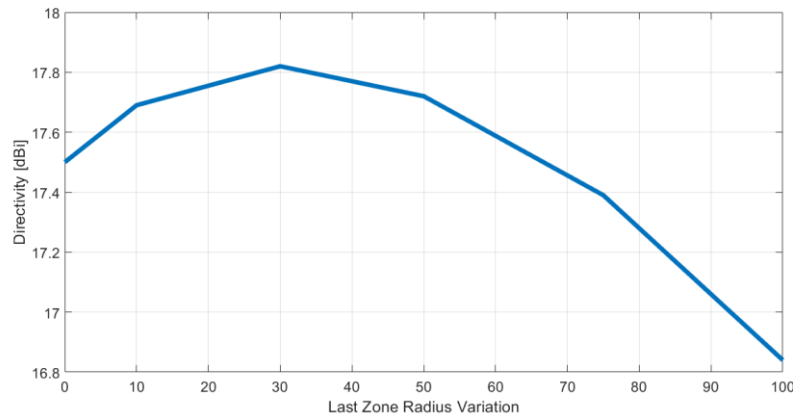


**Figure 14. Evolution of the Directivity with the Last Zone Radius Variation.**

It can be seen that the directivity increases for larger radius until 30 mm in the last radius, that is, a total radius of 828.086 mm.

Figure 15 shows the farfield obtained at that radius length, while Table 5 summarizes the main results of the system.

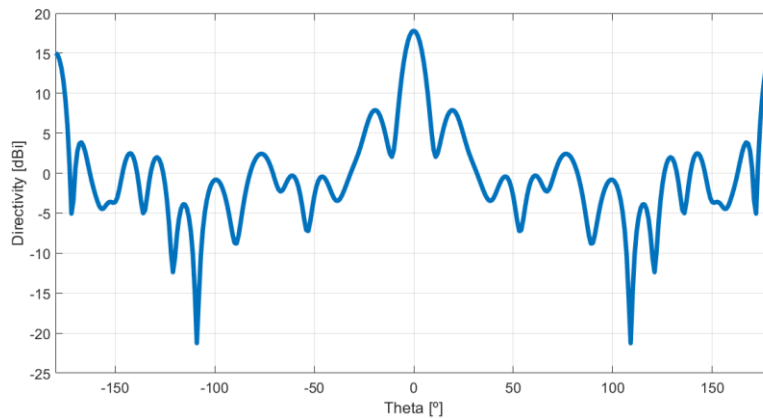


**Figure 15. Radiation Pattern for the 4-zoned Fresnel Zone Plate at 580 mm away of the Feeder and 30 mm more of Radius.**

**Table 5. Simulated Farfield Parameters for the 4-zoned Fresnel Zone Plate at 580 mm away of the Feeder and 30 mm more of Radius.**

| <i>Parameter</i>                  | <i>Result</i> |
|-----------------------------------|---------------|
| <i>Directivity [dBi]</i>          | 17.82         |
| <i>Side Lobe Level. wrp. [dB]</i> | 9.96          |
| <i>F/B Ratio [dB]</i>             | 2.79          |
| <i>Radiation Efficiency [%]</i>   | 94.0          |

Results show that increasing the last radius of the plate, slightly improves the parameters with respect to the original configuration with a distance feeder-plate of 580 mm. Thus, directivity is enhanced 0.32 dBi, and the Side Lobe Level and the F/B Ratio is increased 0.59 dB, and decreased 0.46 dB respectively. On the other hand, the radiation efficiency is slightly increased in a 0.2 %.

Thus, the subsequent analysis will be performed with a 4 Zones plate, 580 mm away from the feeder and with its last radius of 828 mm.

#### 4.2.4. Fresnel Zone Plate – Mass Plane Analysis

In order to increase de directivity, and, above all, reduce the back radiation of the system, two different shape mass plates will be simulated; a square one, and a circular one. Figure 16 shows the simulation of both mass planes.

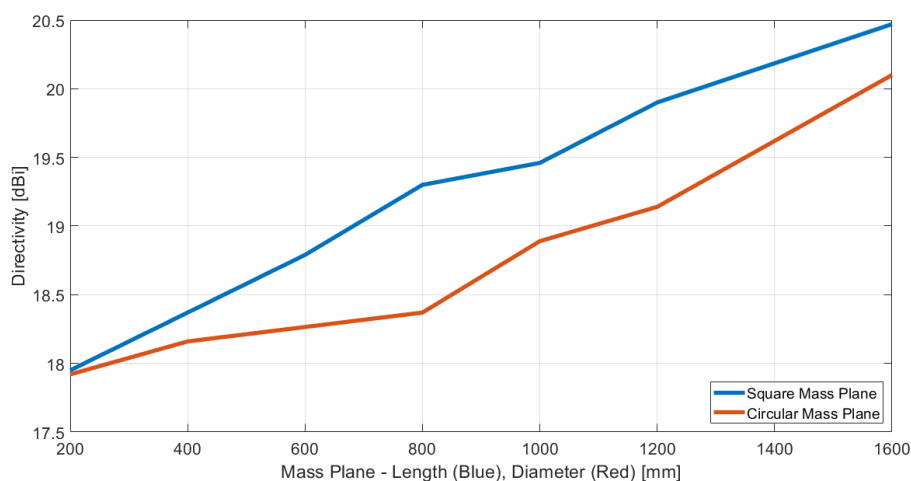


**Figure 16. Evolution of the Directivity with a Mass Plane.**

It can be seen that the square mass plane increases directivity slightly more than the square one. Both, the square and the circular has a fully increasing slope. In order to compare their radiation patterns and their simulated parameters, they will be compared at the point of maximum directivity, that is, a side length of 1600 mm and a diameter of 1600 mm for the square and circular mass plane respectively.

Thus, Figure 17 and Table 6 show the radiation patterns and the farfield parameters respectively.

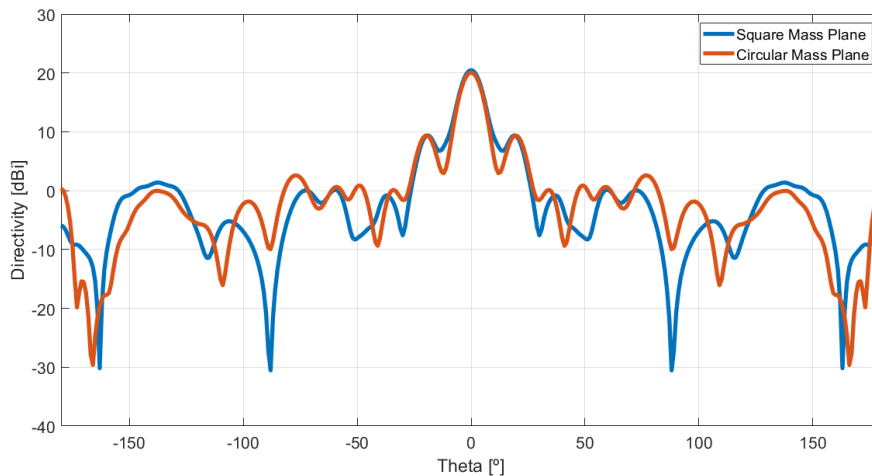


**Figure 17. Radiation Pattern for the 4-zoned Fresnel Zone Plate at 580 mm away of the Feeder and 30 mm more of Radius with Circular/Square Mass Plane**

**Table 6. Simulated Farfield Parameters for the 4-zoned Fresnel Zone Plate at 580 mm away of the Feeder and 30 mm more of Radius with Circular/Square Mass Plane.**

| <i>Parameter</i>                  | <i>Square Mass Plane</i> | <i>Circular Mass Plane</i> |
|-----------------------------------|--------------------------|----------------------------|
| <i>Directivity [dBi]</i>          | 20.46                    | 20.06                      |
| <i>Side Lobe Level. wrp. [dB]</i> | 11.12                    | 10.73                      |
| <i>F/B Ratio [dB]</i>             | 26.37                    | 19.72                      |
| <i>Radiation Efficiency [%]</i>   | 97.4                     | 96.6                       |

Results show differences between both configurations. The square mass plane has better directivity, SLL, and radiation efficiency. In addition, the most important result is the front to back ratio, that is of 26.37 dB for the square mass plane, 23.58 dB better than the last configuration showing that a possible option to reduce the back lobes is using a mass plane.

It is important to remark that a possible reason to explain why the square mass plane offers better performance than the circular one is that the square one has a larger surface.

Thus, the subsequent analysis will be performed with the square mass plane since it offers the best performance.

#### 4.2.5. Fresnel Zone Plate – Serrated Edge Last Zone

Serrated edge reflectors (Figure 19), are a kind of technology that is used to decrease the edge diffraction of reflectors. The diffracted fields, that are the results of the scattered rays that propagate in all directions as, Figure 18 shows, can interact in a destructive way with the radiated main field. Thus, the goal of the serrated edge is redirecting this diffracted fields far away from the main ray. [12]

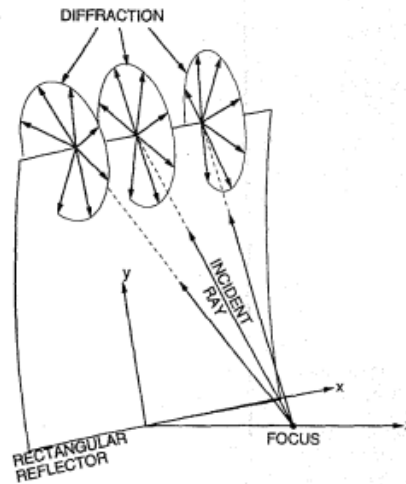


Figure 18. Diffracted Rays from a Reflector [12].

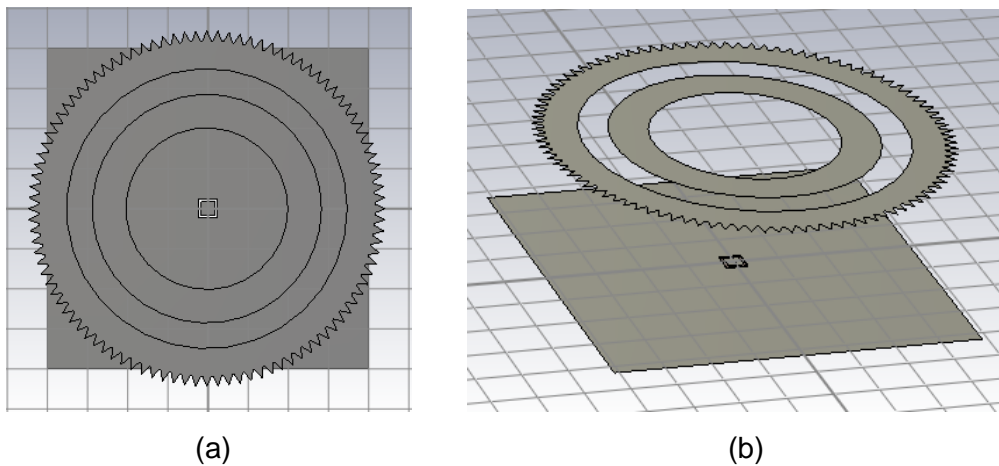
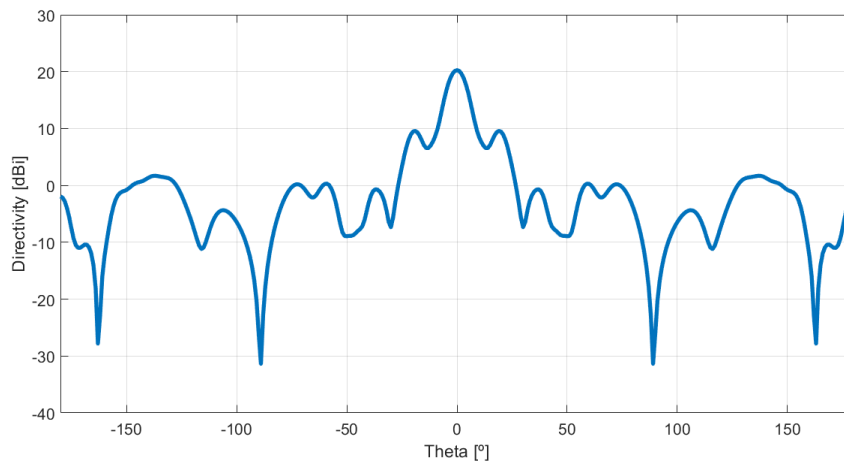


Figure 19. Fresnel Zone Plate with Serrated Edge. (a) Top View. (b) Side View.

Therefore, a serrated edge is implemented in order to improve the properties of the antenna. Results are shown in Figure 20 and Table 7.



**Figure 20. Radiation Pattern for the 4-zoned Fresnel Zone Plate at 580 mm away of the Feeder and 30 mm more of Radius with Square Mass Plane and serrated edge.**

**Table 7. Simulated Farfield Parameters for the 4-zoned Fresnel Zone Plate at 580 mm away of the Feeder and 30 mm more of Radius with Square Mass Plane and serrated edge.**

| <i>Parameter</i>                  | <i>Result</i> |
|-----------------------------------|---------------|
| <i>Directivity [dBi]</i>          | 20.26         |
| <i>Side Lobe Level. wrp. [dB]</i> | 10.07         |
| <i>F/B Ratio [dB]</i>             | 22.20         |
| <i>Radiation Efficiency [%]</i>   | 96.5          |

Results show a slight deterioration in the directivity (0.2 dBi) and in the radiation efficiency (around 1 %), but an important decrease in the SLL (around 1 dB) and over all, in the F/B ratio (around 4dB). Therefore, serrated edges are no implemented.

## 5. Fresnel Zone Plate Antenna Manufacturing

Since the original design is too large, a smaller prototype is created to test the operation of the system. To do this, the antenna is scaled in frequency, in this case at 2.7 GHz.

### 5.1. Scaled Design and Electromagnetic Simulation

Since it is necessary that the dimensions of the antenna be as small as possible, only 2 zones will be taken.

#### 5.1.1. Calculation of Fresnel Zone Radius

- $N = 2$
- $\lambda = \frac{c}{f} = \frac{3 \cdot 10^8}{1.413 \cdot 10^9} = 111.11 \text{ mm}$
- $F_1 = 0.55 \text{ m}$
- $F_2 = 500 \text{ km}$

**Table 8. Prototype Fresnel Zone Radius.**

| n        | 1      | 2      |
|----------|--------|--------|
| $b$ [mm] | 247.20 | 349.60 |

Once obtained the radii of the zones have been obtained, the plate can be performed, being air the even zones and metallic the odd ones in order to obtain a sum in face of all the waves that arrive the plate.

#### 5.1.2. Fresnel Zone Plate Electromagnetic Analysis

Figure 21 shows the farfield obtained, while Table 9 summarizes the main results of the system.

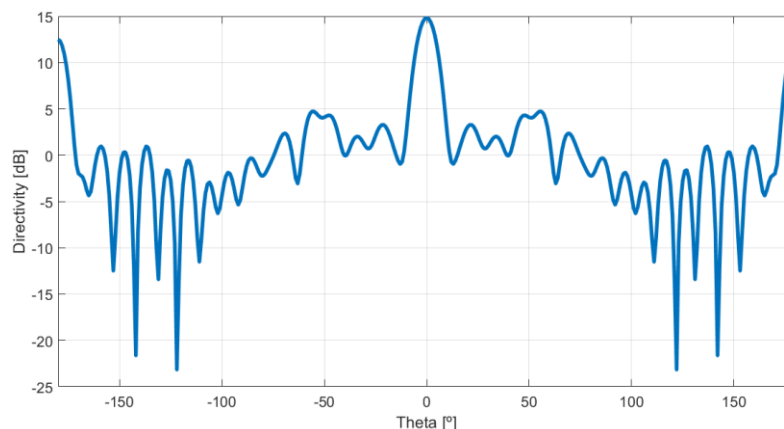


**Figure 21. Radiation Pattern for the Prototype Fresnel Zone Plate.**

**Table 9. Simulated Farfield Parameters for the Prototype Fresnel Zone Plate.**

| <i>Parameter</i>                  | <i>Result</i> |
|-----------------------------------|---------------|
| <i>Directivity [dBi]</i>          | 14.83         |
| <i>Side Lobe Level. wrp. [dB]</i> | 11.55         |
| <i>F/B Ratio [dB]</i>             | 2.50          |
| <i>Radiation Efficiency [%]</i>   | 87.5          |

Once obtained the dimensions of the system it is manufactured in two different ways which share the same structure.

This structure is made by three parts, the base, the carbon fiber rods, and the upper triangle as shown in Figure 22.

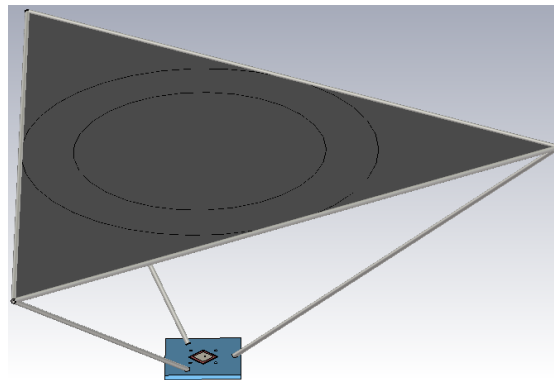


**Figure 22. Fresnel Zone Plate Structure Design.**

## 5.2. Base Design

The base (Figure 23) is manufactured with a 3D printer. It has a square shape with four holes spaced 50 mm. These holes are used to anchor the system to the rotor of the anechoic chamber with m6 screws in order to analyse the operation of the antenna.

In addition, the base has a slot where the feeder fits and a hole where the probe passes.

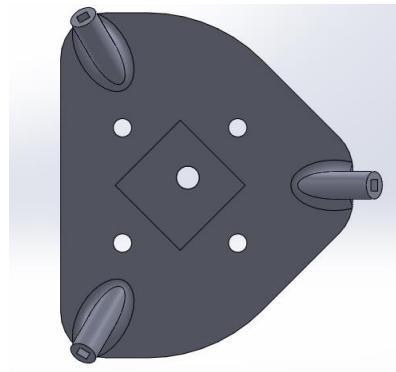


**Figure 23. Elevation of the Base.**

### 5.3. Rod Placement

There are two types of rods, both made of carbon fiber. The first type has 788.16 mm of length, and it is anchored at one end to the base with an angle of 54.29 degrees from the vertical in order to place each vertex of the triangle at the desired distance (460 mm).

On the other hand, the second type of rods has a length of 1212 mm and are used to build an equilateral triangle forming a pyramid that gives stability to the structure.

The two types of rods are joint by a piece created by a 3-D printer, which is shown in Figure 24.

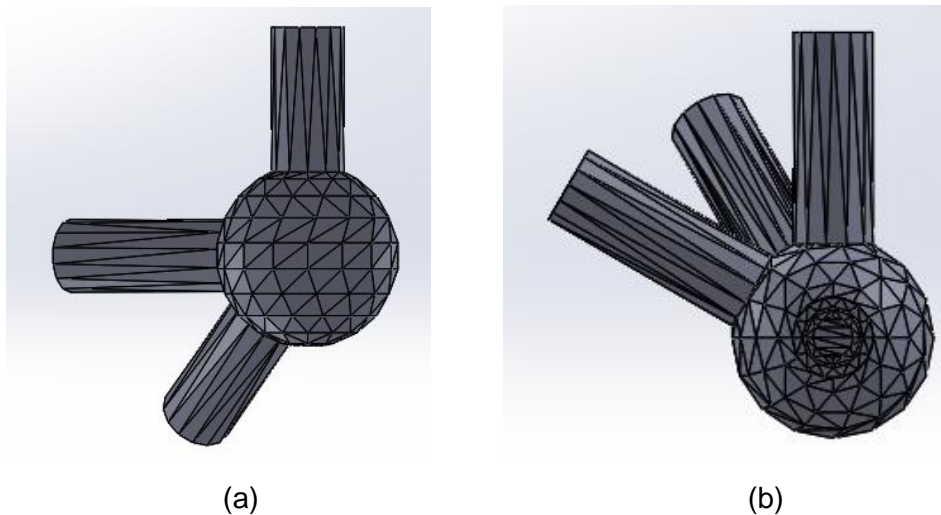


**Figure 24. Views of the Union. (a) Side View. (b) Top View.**

Thus, it can be seen that there are two horizontal parts in order to form the triangle. Furthermore, it can be appreciated an inclined part to join the upper triangle structure with the base. Finally, a vertical part is used to join the upper triangle with the piece union.

### 5.4. Upper Triangle

Finally, the circle that forms the crown will be inscribed in a triangle of 1212 mm of side that is nailed to the upper part of the joining pieces and the rods. Two different options are implemented:

#### 5.4.1. Configuration A

Figure 25 shows the first implemented triangle. It is a 20 mm thick polystyrene triangle. As conductor material for the Fresnel Zones, an anti-radiation paint will be used (Figure 26). In addition, it can be appreciated that a circular section has been removed from the centre of the triangle in order to make it lighter and allow the air to pass through the antenna without the antenna acting like a ship sail. The final assembly is shown in Figure 26.



Figure 25. Upper Polystyrene Triangle.



Figure 26. Configuration A - Assembled Antenna

#### 5.4.2. Configuration B

On the other hand, the second option only differs from the first one in two aspects; on the one hand, the upper polystyrene triangle is exchanged by a plastic cloth. On the other hand, the conductor material is modelled with silver duct tape. This way, the base, the rods and their joint can be reused. The final assembly is shown in Figure 27.



Figure 27. Configuration B - Assembled Antenna

## 6. Electromagnetic Measurements

### 6.1. Feeder Electromagnetic Measurement

The first measured element of the system was the feeder. It was measured with a network analyser (Figure 28) which is previously calibrated with a calibration kit. Results are shown in Figure 29.

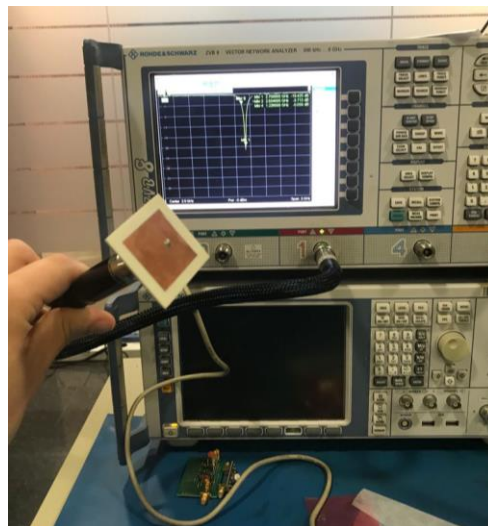


Figure 28. Feeder Measurement.

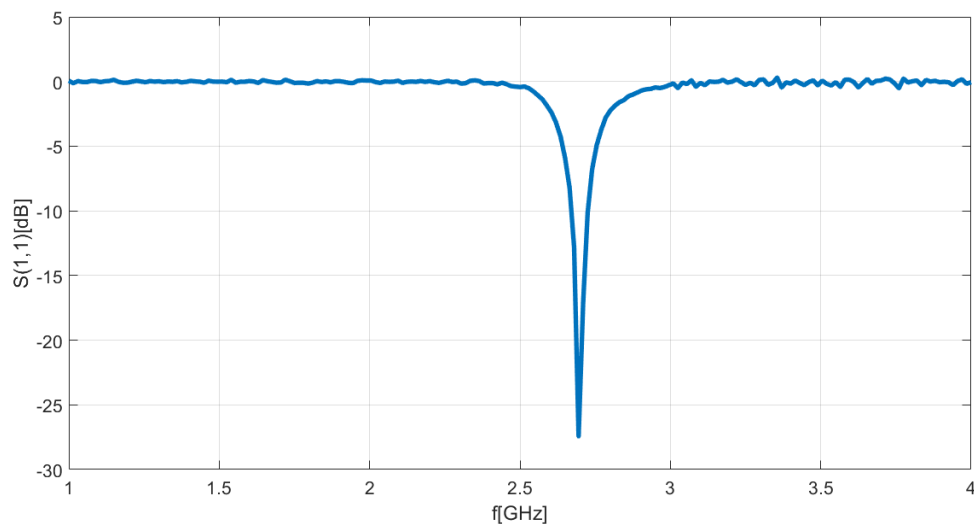


Figure 29. Feeder Measurement Results.

From the measurement, it is obtained an adaptation smaller than -10 dB over a bandwidth of 60 MHz.

After measuring the feeder, both configurations of the FZP antenna were measured in the UPC AntennaLab anechoic chamber.

## 6.2. Configuration A - Measurement

Figure 30 shows the system anchored to the chamber rotor, while Figure 31 and Table 10 show the electromagnetic results.

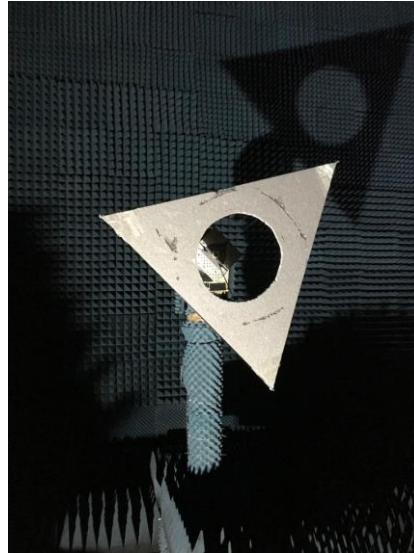


Figure 30. Configuration A – Antenna Anchored in the Chamber

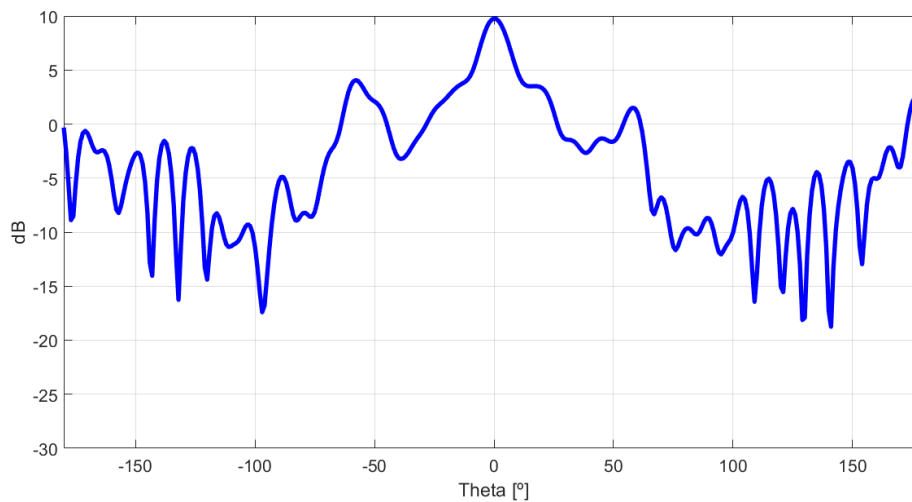


Figure 31. Configuration A – Antenna Pattern Measurement

Table 10- Configuration A – Antenna Pattern Measurement Parameters Results

| <i>Parameter</i>                  | <i>Result</i> |
|-----------------------------------|---------------|
| <i>Directivity [dBi]</i>          | 9.70          |
| <i>Side Lobe Level. wrp. [dB]</i> | 5.64          |
| <i>F/B Ratio [dB]</i>             | 7.25          |

### 6.3. Configuration B - Measurement

Figure 32 shows the system anchored to the chamber rotor, while Figure 33 and Table 11 show the electromagnetic results.

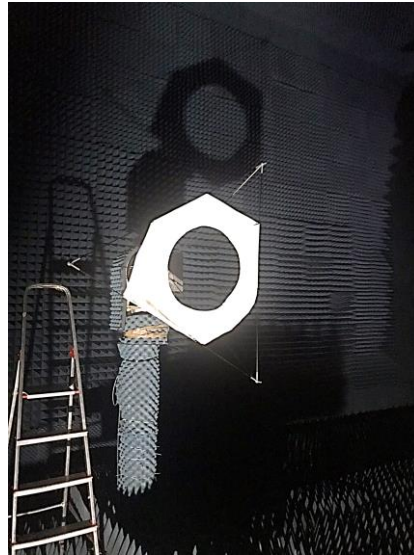


Figure 32. Configuration B – Antenna Anchored in the Chamber

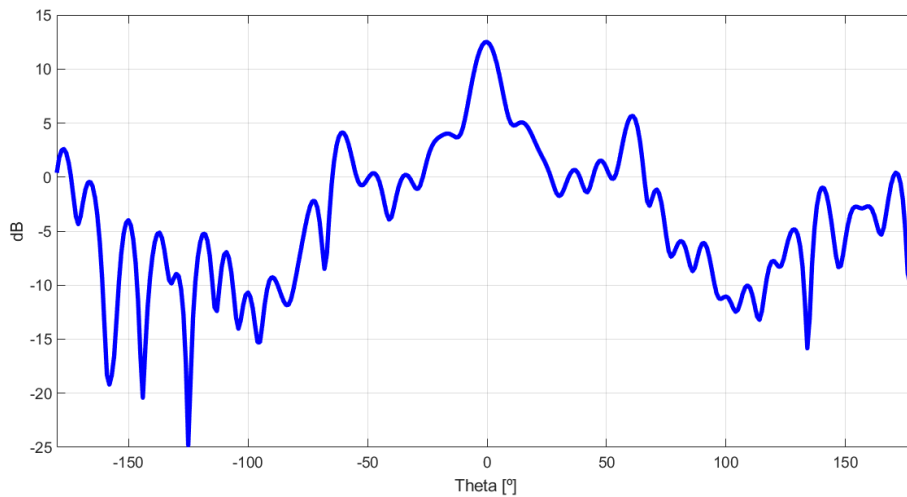


Figure 33. Configuration B – Antenna Pattern Measurement

Table 11- Configuration B – Antenna Pattern Measurement Parameters Results

| Parameter                  | Result |
|----------------------------|--------|
| Directivity [dBi]          | 12.51  |
| Side Lobe Level. wrp. [dB] | 6.84   |
| F/B Ratio [dB]             | 12.11  |

## 7. Conclusions

### 7.1. Electromagnetic Conclusions

Figure 34 and Table 12 shows a comparison of the electromagnetic simulations and both configurations measurements.

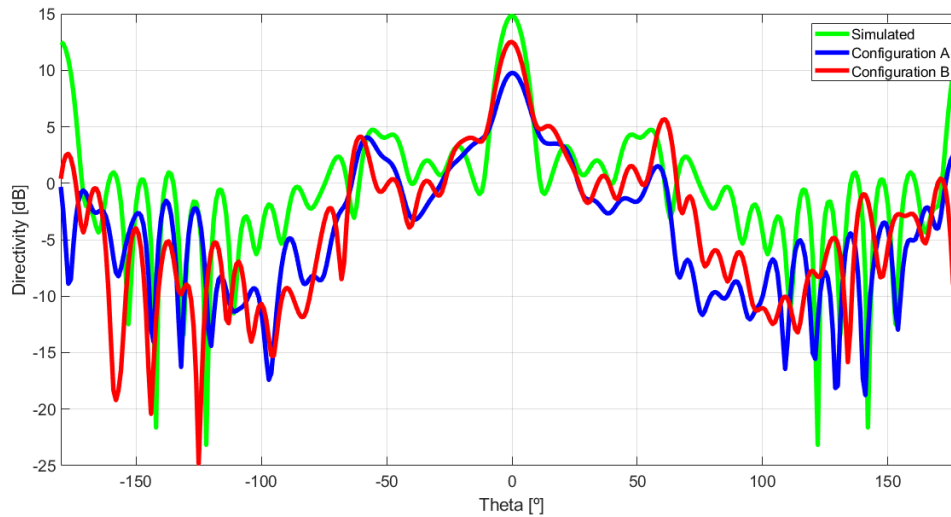


**Figure 34. Electromagnetic vs Measurement Farfield Results**

**Table 12- Electromagnetic vs Measurement Parameters Results**

| <i>Parameter</i>                  | <i>Electromagnetic Simulation</i> | <i>Configuration A</i> | <i>Configuration B</i> |
|-----------------------------------|-----------------------------------|------------------------|------------------------|
| <i>Directivity [dBi]</i>          | 14.83                             | 9.70                   | 12.51                  |
| <i>Side Lobe Level. wrp. [dB]</i> | 11.55                             | 5.64                   | 6.84                   |
| <i>F/B Ratio [dB]</i>             | 2.50                              | 7.25                   | 12.11                  |

On the one hand, directivity comparison shows that the simulated results are the higher ones as expected. Then, Configuration B offers the best tested directivity, almost 3 dB over Configuration A, and less than 3 dB under the simulated one.

On the other hand, tested SLL results are worse than the simulated ones, being better the Configuration B result.

Difference between simulated and tested results are reasonable since the simulated ones are made in ideal conditions, without the human factor that may introduce errors. Moreover, the metallic zones are performed as PEC (Perfect Electric Conductor) in the simulation, while, in the manufactured antennas, the metallic zones where performed with no ideal materials.

Finally, the front back ratio is better for the manufactured antennas, being the Configuration B one almost 5 dB over Configuration A, and almost over 10 dB of the simulation. The improvement of this ratio in the manufactured antennas is caused due to the fact that the metallic zones are no ideal, allowing part of the radiation pass through them, losing directivity, but enhancing the F/B ratio. On the other hand, since the simulation where

performed with PEC, all the radiation bounced off the metal areas increasing the back lobe. Nevertheless, as section 4.2.4 shows, the F/B can be highly improved using a mass plane so that the back lobes will bounce off it.

Comparison between Configuration A and B results may be caused by several reasons:

- Manufacturing errors: Since both antennas were manufactured, it is possible that one configuration is made more precisely than the other.
- Upper Triangle: The upper triangle of Configuration A was bigger and slightly heavier than the Configuration B one. This structural difference could cause vibrations in the system when the rotor of the anechoic chamber turned.
- Metallization: It is possible that the materials used to metallize the zones behave differently. Thus, both materials were measured. The setup is made with a VNA and a horn whose opening is covered with a sheet of each material. It is important to remark that the VNA must be calibrated as in point 6.1, to obtain the results of Figure 35.

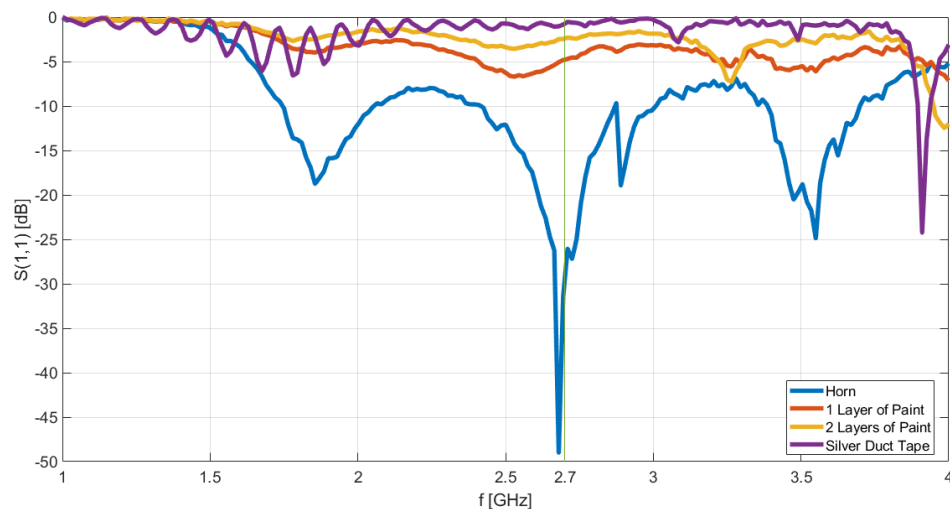


**Figure 35. Metallic Material Comparison**

First of all, it can be seen that the horn is perfectly matched at 2.7 GHz. On the one hand, if a sheet painted with the Configuration A paint is used to cover the opening of the horn, the matching has a value of around -4.9 dB. In addition, if two sheets of the same material are used, the matching decreases to -2.5 dB. On the other hand, using the silver duct tape of Configuration B offers a matching of -1 dB, less than 3 dB than Configuration A, where one painted sheet is used.

Thus, it could be said that one of the reasons for the difference between Configuration A and B is the metallic material.

## 7.2. Future Lines

Next step in the research is trying to improve the F/B ratio mixing both materials, that is using the silver duct tape and then, painting the system, which, due to the absorbent properties of the paint, should offer an improved front to back ratio.

Other future line is manufacturing, with the help of the members of the UPC Nanosat Lab, the original L-Band deployable antenna with the deployment mechanism.

Finally, it would be interesting to keep deepening in the serrated edge concept since each zone introduces two diffraction zones, its inner and outer radius in order to improve the efficiency of the system. Thus, each border zone should be serrated edged.

### 7.3. Learned Lessons

Throughout the Project, several concepts unrelated to the project have been learnt:

- The importance of choosing a good electromagnetic software setup (in this case CST) before performing the simulations.
  - On the one hand, it is really important to select a solver that suits what you want to simulate. In this project 2 different solvers were used:
    - Integral Equation Solver: This solver offers the option “Farfield Source”, that allows the user to import and allocate a certain farfield exported from other file. Despite this solver allow faster simulations, it gives unreal results since all the structure of the feeder is completely ignored.
    - Time Domain Solver: This is the one used in the project since it is very useful to simulate large structures. It uses FDTD method to solve the maxwell's equations.
  - On the other hand, it is, as important as the solver, choosing a correct mesh. The mesh used in the project was the hexahedral mesh, which is the one where the computational volume is discretized by means of rectangular cuboids of variable size called mesh cells. Thus, each mesh cell will be the volume in which the electric and magnetic fields are calculated. Therefore, the more mesh cells we use, the more accurate simulations will be obtained. In this project, a large mesh (few large mesh cells) was used at the beginning, since it was desired to see roughly how the system worked. Later a small mesh (many small mesh cells) was used, to obtain more precise results.
- Another aspect that has been learned is choosing the appropriate materials in the manufacturing of the system, both mechanically and electromagnetically. On the one hand, the size and weight of all the materials have been taken into account, especially the rods, in order to obtain a resistant, light structure, and without buckling in the anechoic chamber. On the other hand, the importance of the material in the metallization of the areas has been verified from the electromagnetic point of view, since as it has been shown, using one material or another one drastically changes the performance of the antenna.
- Preparation of the antenna to measure in anechoic chamber. Since this is the first time that I have measured in an anechoic chamber, I have learned that a support must be specially designed to anchor the antenna to the chamber rotor, in addition to the importance of making a resistant and light antenna to avoid unwanted movements when it rotates system in the measurement.
- As a last point to highlight, it is the first time that a 3D printer is used, I have learned how to use it, and how to design the parts with the appropriate software.

## 8. Budget

In the budget, only the manufacture and measurement process of the antennas is quantified, since all the licences of the software used in the design and simulation of them have been free of charge student licenses.

**Table 13. Materials Budget**

| Material             | Quantity | Unit Price [€] | Total [€] |
|----------------------|----------|----------------|-----------|
| Fiber Rods (1,5 m)   | 5        | 7              | 35        |
| Fiber Rods (2 m)     | 5        | 8,02           | 40,1      |
| Circular Vinyl       | 2        | 17             | 34        |
| Anti-radiation Paint | 1        | 20,5           | 20,5      |
| Polystyrene Triangle | 1        | 42,15          | 42,15     |
| Silver Duct Tape     | 2        | 20             | 40        |
| Total                |          |                | 211,75    |

**Table 14. Measurement Equipment Budget**

| Concept          | Year Price [€/year] | Day Price [€/h] | Days Used | Total Price [€] |
|------------------|---------------------|-----------------|-----------|-----------------|
| VNA              | 7000                | 19.17           | 4         | 76.68           |
| Anechoic Chamber | 438000              | 1200            | 2         | 2400            |
| Total            |                     |                 |           | 2476.88         |

Finally, salary of the engineers is broken down in Table 15.

**Table 15. Engineers Salary Break Down**

| Nº Engineers | Salary [€/h] | Time (1day=8h) [h] | Total [€] |
|--------------|--------------|--------------------|-----------|
| 1            | 10           | 109 x 8 =872       | 8720      |

The budget of the whole project is:

**Table 16. Budget of the Whole Project**

| Concept               | Price [€] |
|-----------------------|-----------|
| Materials             | 211,75    |
| Measurement Equipment | 2476.88   |
| Salary                | 8720      |
| Total                 | 11408.63  |

## 9. Gantt Diagram

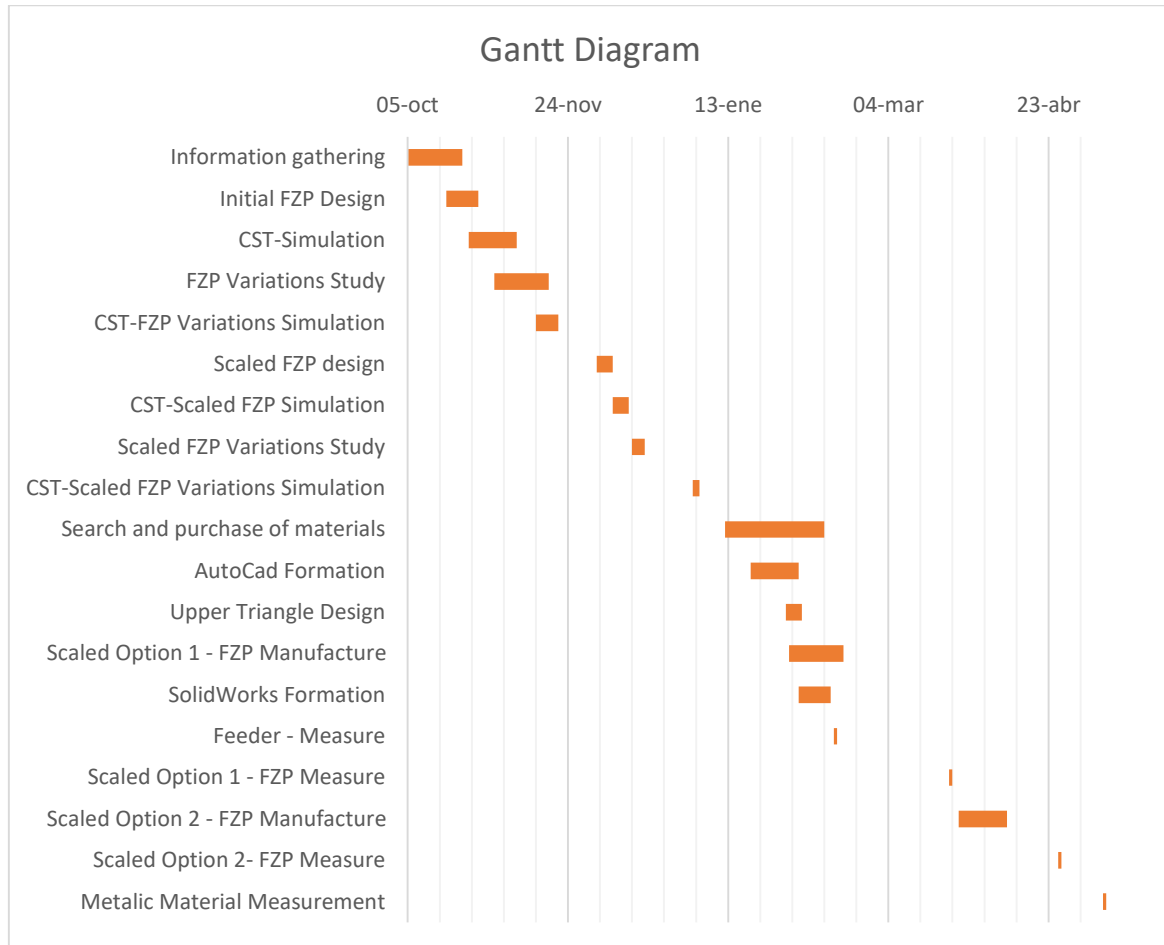


**Figure 36. Gantt Diagram**

The first task was gathering information, in order to create a general background and to define the state of the art, reviewing several articles and books. Afterwards, the design of the first 20-zoned antenna, which was simulated using the electromagnetic software, CST [11], was performed.

Once obtained the results, current advances and developments in the field were studied and simulated in order to improve the operation and performance of the antenna.

However, due to the large size of the resulting antenna, it was decided to repeat the process for a smaller frequency-scaled antenna, which was manufactured following two configurations with different materials. For the design of the necessary parts for the structure of the antenna, training in Autocad and Solidworks was necessary.

Once the patch was manufactured, it was measured with a network analyzer, while both configurations of the antennas were tested in an anechoic chamber.

Finally, in order to better understand the results, the metallic materials were measured with a network analyzer.

It is important to remark that the project should be finished in January. Nevertheless, the fact of starting an internship in the company SENER Aeroespacial forced to distribute the time between project and practices, lengthening the duration of the project.

## **Bibliography**

- [1] The CubeSat Standard. [Online] Available: <https://www.cubesat.org/cubesatinfo> [Accessed: 29 December 2020].
- [2] Auriga Mission. [Online] Available: <https://www.nanosats.eu/sat/auriga> [Accessed: 29 December 2020].
- [3] NASA ATS-6 Mission. [Online] Available: <https://www.nasa.gov/centers/goddard/missions/ats.html> [Accessed: 29 December 2020].
- [4] Jose Nieto Mocholi, Saniel Valcázar, Aitor Martínez, Adriano Camps, Florian Deconinck. "LARGE DEPLOYABLE OFFSET FED ANTENNAS FOR CUBESATS". *40<sup>th</sup> ESA Antenna Workshop – Antenna Developments for Terrestrial and Small-Space Platforms. 8-10 October 2019, Noordwijk, The Netherlands.*
- [5] NanoSat Lab. [Online] Available: <https://nanosatlab.upc.edu/en> [Accessed: 29 December 2020].
- [6] M. Mendez-Soto, A. Márquez-Alperi, E. Fernández-Niño and A. Camps, "Parametric Analysis of an L-Band Deployable Offset Reflector for CubeSats," in *IEEE Journal on Miniaturization for Air and Space Systems*, vol. 1, no. 1, pp. 66-73, June 2020, doi: 10.1109/JMASS.2020.3002339.
- [7] James C. Witse. "History and Evolution of Fresnel Zone Plate Antennas for Microwaves and Milimeter Waves".
- [8] Bell Telephone Labs. [Online] Available: <https://www.bell-labs.com/> [Accessed: 29 December 2020].
- [9] L. Van Buskirk and C. Hendrix, "The zone plate as a radio-frequency focusing element," in *IRE Transactions on Antennas and Propagation*, vol. 9, no. 3, pp. 319-320, May 1961, doi: 10.1109/TAP.1961.1144988.
- [10] Huygens' Principle. [Online] Available: <http://hyperphysics.phy-astr.gsu.edu/hbase/phyopt/huygen.html> [Accessed: 29 December 2020].
- [11] CST Studio Suite. [Online] Available: <https://www.3ds.com/es/productos-y-servicios/simulia/productos/cst-studio-suite/> [Accessed: 29 December 2020].
- [12] Teh-Hong Lee and W. D. Burnside, "Performance trade-off between serrated edge and blended rolled edge compact range reflectors," in *IEEE Transactions on Antennas and Propagation*, vol. 44, no. 1, pp. 87-96, Jan. 1996, doi: 10.1109/8.477532.



## Glossary

FZP: Fresnel Zone Plate.

PEC: Perfect Electric Conductor.